Review | Vol. 9, No. 3 | 1 Mar 2019 | OPTICAL MATERIALS EXPRESS 1136
Optical Materials EXPRESS

Second harmonic generation spectroscopy on two-dimensional materials [Invited]

YING WANG,[1] JUN XIAO,[1] SUI YANG,[1] YUAN WANG,[1] AND XIANG ZHANG[1,2,*]

[1]NSF Nanoscale Science and Engineering Center (NSEC), 3112 Etcheverry Hall, University of California, Berkeley, CA 94720, USA
[2]University of Hong Kong, Hong Kong, China
[*]xzhang-me@berkeley.edu

Abstract: The discovery of atomically thin layered materials such as graphene and transition metal dichalcogenides has unveiled the unique exploration of novel fundamental physics and device applications in two-dimensions. Characterization of their crystal symmetry and subsequent electronic properties are prominent to realize the full potential of these reduced dimensional systems, which fundamentally determine the topology, chirality and rich interfacial physics. Second harmonic generation (SHG), a nonlinear optical effect, is sensitive to crystal symmetry and electronic structures, which proves to be one of the most powerful yet simple technique to capture the essence physics. On the other hand, the 2D nature of layered materials enables large tunability in its physical properties with a number of external stimuli, which in turn paves the way for the development of 2D nonlinear optoelectronic applications. In this review, we overview recent efforts employing second harmonic generation spectroscopy and microscopy to probe lattice structures and dipole polarizations in two-dimensional transition metal dichalcogenide and polar materials. In addition, multiple external stimuli used to control SHG as potential optoelectronic devices are covered. We conclude with a perspective on the future directions of exploration on emerging 2D magnetic and topological materials based on SHG spectroscopy.

1. Introduction

Two-dimensional (2D) materials have been intensively studied since the discovery of graphene. Because its unique mechanical, electric and optical properties and its special linear-Dirac dispersion, graphene not only exhibits novel physics [1], but also is proved to be an excellent platform for various applications from thermal conductors to optical modulators [2–7]. And the family of 2D materials grows fast and features more than 150 layered materials that can be mechanically exfoliated down to monolayer with sub nm thickness. Among them, transition metal dichalcogenides (TMDs) occupy a large population. Unlike graphene, 2D TMDs cover the whole electrical conductivity spectrum from metals, semi-conductors to insulators [8], making the ultra thin and low power transistors possible [9]. Moreover, hexagonal (2H) TMDs with inversion symmetry breaking show inequivalent valleys at the corners of the Brillouin zone, leading to new valley degree of freedom [10–12]. Furthermore, the strong quantum confinement in atomic scale makes the optical properties of 2D materials sensitive to layer numbers from monolayer to bulk [13–15]. For example, the electronic band structures of 2D materials strongly depend on the layer numbers. The band gap of 2H-TMDs changes from indirect to direct transition as the thickness of flakes changes from multilayers to monolayers [16]. And the band gap increases more than 1 eV as the quantum confinement are taken into account when thickness of black phosphorus is atomic [17,18]. Moreover, the individual layers usually have symmetry distinct from their bulky counterpart. Few-layer materials of different layer number can have different symmetries from one another, even though their thickness differs by only one atomic layer. And nowadays, one artificial stacking

#348467 https://doi.org/10.1364/OME.9.001136
Journal © 2019 Received 22 Oct 2018; revised 16 Dec 2018; accepted 16 Dec 2018; published 12 Feb 2019

Optical Materials EXPRESS

heterostructure can be designed with arbitrary angles hence results in large variance of symmetries [19–21]. Such variety leads to booming engineering of materials' properties.

However, atomic thickness of layered materials makes the sample characterization become challenging because signal decreases for thinner samples. Hence, clean surface or high vacuum becomes necessary for most of characterization tools. Second Harmonic Generation (SHG) stands out as one attractive characterization approach because of it simplicity, versatility and non-contact ability [22]. More specifically, pulse-laser excitation of SHG makes this technique very unique as remote sensing since the SHG from surface is highly directional. If combining with a pulse-laser probe, it is also potential to use SHG to monitor the fast dynamic change of those monolayers [23].

SHG as a second-order nonlinear optical process is only allowed in a material with inversion symmetry breaking [22]. Consider an optical wave with a frequency ω, passing through a material (Fig. 1(a)). The wave-induced dipoles can behave like anharmonic oscillators, which oscillate at the frequency $2\omega, 3\omega$ and so on and radiate electromagnetic (EM) waves accordingly. In the SHG spectroscopy, we specifically focus on the EM wave with frequency 2ω. And quantitatively the induced dipole component $P^{(2)}(2\omega)$, as the source of the second harmonic radiation, is determined by $\chi^{(2)}\mathrm{E}^2(\omega)$, where $\chi^{(2)}$ is the nonlinear susceptibility. Considering one material has inversion symmetry, the excitation fields $\mathrm{E}(\omega)$ and $-\mathrm{E}(\omega)$ will induce the dipoles $P^{(2)}(2\omega)$ and $-P^{(2)}(2\omega)$ respectively. The relation between induced dipole and excitation filed cannot be built unless the $\chi^{(2)} = 0$. Hence the SHG is zero and forbidden for centrosymmetric materials.

The measurement setup for SHG is fairly simple. The excitation of ω frequency is generally pulsed laser so that power is enough for anharmonic excitation. The SHG which is the double frequency differs itself from the excitation so that one can filter the signal out of the excitation easily. In the following, we discuss the applications of SHG to layered materials in the perspectives of revelation of in-plane symmetry, layer-thickness dependence, stacking orders, and out-of plane polarity as well as its unique optical and electrical tunability in two-dimensional materials.

Optical Materials EXPRESS

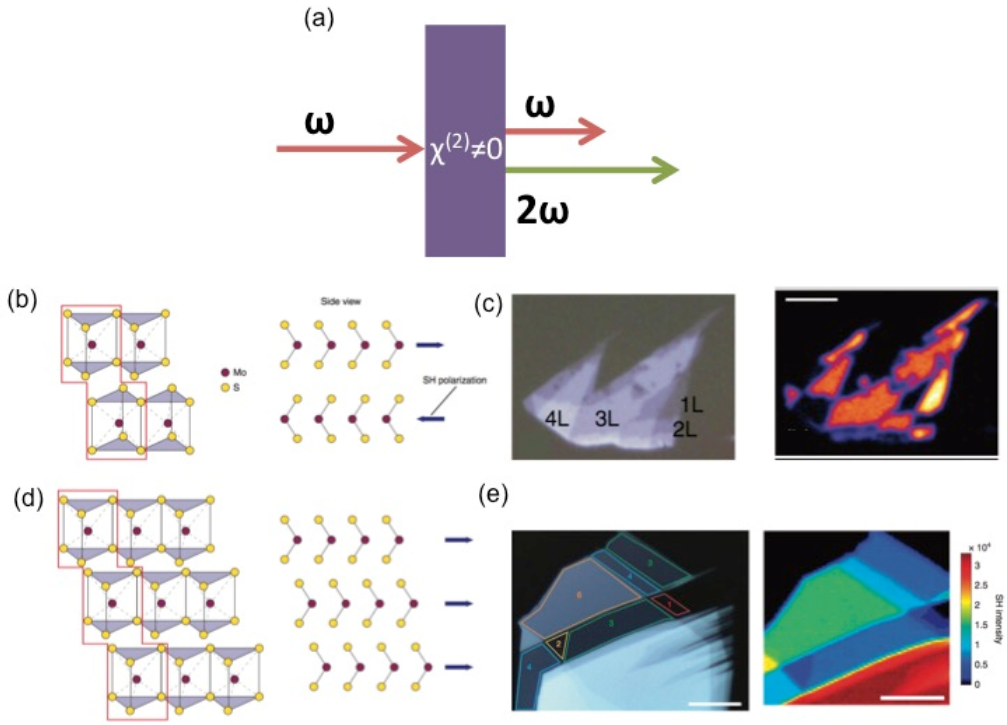

Fig. 1. (a) Schematic of the generation of second harmonic generation in non-centrosymmetric materials, in which frequency of excitation is half of the generated light. (b) In 2H-MoS_2, the Mo atoms are hexagonally packed within each layer and trigonal prismatically coordinated with S atoms on the top and bottom. The side projection shows the flipped orientation of each layer and the anti-parallel orientation of the SH dipoles. In (c), the absence of SHG in even layers exhibits the cancellation of SH dipoles. (d) Crystal structure of 3R-MoS_2 (trilayer unit cell outlined in red). Individual layers are identical to the 2H structure, however the unit cell and bulk crystal are noncentrosymmetric. The layers are oriented in such a way that the dipoles are parallel allowing for constructive interference of SHG in (e). (b), (d), (e) are reprinted from ref [24]with permission from Springer Nature and (c) is adapted from ref [25] with permission from American Physical Society.

2. SHG characterization of layered TMDCs and their heterostructures

As one important member in layered materials, ultrathin group VI transition metal dichalcogenides (MX_2, M = Mo,W; X = S, Se, Te) have gained prominent attention because of many unique properties such as the emerging photoluminescence [26,27], excellent transistor on-off ratio [9], optical valley polarization [11,28], large exciton and trion binding energies [29,30], superconductivity [31] and piezoelectricity [32,33]. In addition, multiple crystal structure forms like 2H, 1T', T_d phase coexist and some of which are even under topological protection. Most of these significant features originate from their layer-dependent crystal symmetry, which can be easily revealed by SHG. In this section, application of SHG to explore layer-dependent crystal symmetry in 2H and 3R TMDs, stacking angle in artificial heterostructures as well as polarized pattern are discussed.

2.1. Layered dependent symmetry breaking and preservation in single crystalline TMDs

The most commonly studied bulk crystal phase of MX_2 is the 2H polytype, with two X–M–X unit cells of trigonal prismatic coordination and space group D_{6h} (Fig. 1(b)). For odd layers, the lack of inversion symmetry gives rise to a finite second-order nonlinearity and SHG

Optical Materials EXPRESS

intensity, which is absent in even layers [25] (Fig. 1(c)). Such layer-dependent SHG in 2H MX_2 can be also understood by the coherent interference effect. In single layer of MX_2, the nonlinear susceptibility is a finite number but alternative sign in adjacent layers due to AB stacking. For nanoflakes with even layer number, the SHG signals from adjacent layers are cancelled out. Hence, high contrast of SH intensity between odd and even numbers can be used to characterize parity of layer number. For odd layers of MX_2 with finite SHG, the exact layer number is further identified by intensity variation of SHG with layers number [34].

In contrast to AB stacking in 2H phase, in which the even layers restore the inversion symmetry, the layers in the 3R phase remain the same orientation and shift along the in-plane direction (Fig. 1(d)). The dipoles are parallel to allow for constructive interference of SHG, resulting in quadratic increase of second-harmonic intensity with more layers [24] (Fig. 1(e)). This finding also verified the atomically phase-matching in 2D crystals. While in 1T' phase form, the trend of layer dependent SHG is opposite to that in 2H phase. In other words, even layers of 1T' crystal with inversion symmetry breaking display significant SHG while odd layers with inversion symmetry show negligible SHG [35]. Therefore, the stacking sequence of 2D materials plays a very important role in determining the preservation or breaking the inversion symmetry in atomically thin crystals and corresponding SHG intensity.

2.2. SHG characterization of twisted angles in artificial TMDs heterostructures

Moreover, designed vertical stacking of TMDs heterostructures with specific twisted angles creates new material system with tailored properties [36,37].Given the atomic phase-matching condition, SHG from the artificial heterostructure can be regarded as a coherent superposition of the SH fields from the individual layers [38], with a phase difference depending on the stacking angle (Fig. 2(a)-2(d)). The linearly polarized SH fields for each layer is generated through the linear polarized fundamental excitation field. The total SH electric field $\vec{E}_s(2\omega)$ in the stacking region is the vector superposition of electric field in each layer: $\vec{E}_s(2\omega) = \vec{E}_1(2\omega) + \vec{E}_2(2\omega)$. Hence, the total SH intensity from the stacking region is proportional to $\left|\vec{E}_s(2\omega)\right|^2$, expressed as $I_s(\theta) = I_1 + I_2 + 2\sqrt{I_1 I_2}\cos(3\theta)$, where I_s, I_1 and I_2 stand for the SH intensities from the stacking region, the monolayer flake 1, and flake 2, respectively; and $\theta = \varphi_1 + \varphi_2$ is the stacking angle, which is defined as the angle between two nearest perpendicular bisectors (armchair directions) of the two triangular flakes. Because of the variance of SHG intensity among different flakes, people define a dimensionless parameter $\kappa(\theta) = (I_s - I_1 - I_2)/2(I_1 I_2)^{1/2}$ and verified the $\cos(3\theta)$ dependence. Therefore, by building the relationship between SHG intensities from stacking and bare regions, the angle of stacking can be easily resolved without any damage to materials.

With the same interference principle for electric fields from different layers, researchers take advantage of the SHG destruction to identify domain walls in 2D materials as well. For instance, polycrystalline flakes with in-plane stitched patches are commonly obtained from CVD synthesis. Destructive interference occurs when neighboring domains grow with opposite dipoles or orientation mismatch, resulting in dark line referring to domain walls [39]. Such visualization of crystal grain boundaries provides key information for optimization of single crystallization in CVD growth.

Optical Materials EXPRESS

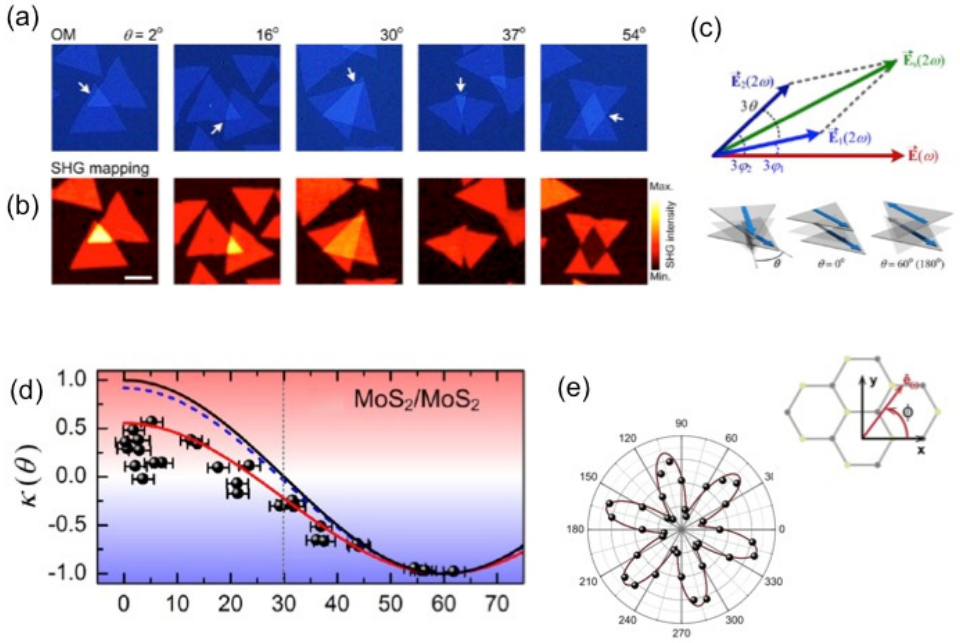

Fig. 2. (a) Optical microscopy images for a series of MoS_2 bilayers with a stacking angle distributed from θ = 0° to 60°. (b) The corresponding false color-coded SH intensity mappings of flakes shown in (a). The scale bar is 5 μm. (c) A schematic for illustrating the vector superposition of the SH electric fields, where $\vec{E}(\omega)$ is the electric field of the fundamental light, $\vec{E}_1(2\omega)$ ($\vec{E}_2(2\omega)$) is the SH electric field from the flake 1 (flake 2), and $\vec{E}_s(2\omega)$ is the resulting SH electric field from the stacking region. In the insets of (c), schematics for stacked bilayers with specific θ = 0°, 60° or 180°. (d) The measured angular dependence of κ(θ) for homogeneous MoS_2/MoS_2 bilayers. (e) Polar plot of the second-harmonic intensity from monolayer MoS_2 as a function of the sample angle. And the inset shows top view of the MoS_2 crystallographic orientation with respect to the incident laser polarization. Yellow and gray dots refer to S and Mo atoms respectively. (a)-(d) are adapted with permission from ref [38]. Copyright 2014 American Chemical Society. (e) is reprinted from ref [25] with permission from American Physical Society.

2.3. Polarized SHG identifies crystal orientation

Considering the fabrication of a heterostructure with specific requirement of stacking angle, the knowledge of crystal orientation is fundamental as the first step. Polarized SHG establishes a relation with the sample's rotation angles and works as a precise optical probe of the orientation of the crystallographic axes [34]. Essentially an analyzer was used to select the polarization components of the SH radiation lying either parallel or perpendicular to the polarization of the pump beam. The working principle for this method is described below and we take the monolayers of 2H TMDs as an example. Exfoliated monolayers of 2H TMDs belong to the D_{3h} symmetry group, which gives only one independent nonvanishing element of the nonlinear response: $\chi^2_{MoS_2} = \chi^2_{xxx} = -\chi^2_{xyy} = -\chi^2_{yyx} = -\chi^2_{yxy}$, where x corresponds to the armchair direction and y is the zigzag direction. And the electric field of the generated second-harmonic light $\vec{E}(2\omega)$ along a given direction $\vec{e}_{2\omega}$ can be described in terms of the

Optical Materials EXPRESS

$\chi^{(2)}$ tensor and input light polarization vector $\vec{e}_\omega$ as $E(2\omega) \bullet \vec{e}_{2\omega} = C\vec{e}_{2\omega} \bullet \chi^{(2)} : \vec{e}_\omega \vec{e}_\omega$, where ω is the laser frequency, 2ω is the SH frequency, and C is a proportionality constant which contains local-field factors determined by the local dielectric environment. For a pump-laser polarization parallel or perpendicular to the polarization of the input laser, the generated second-harmonic electric field is expressed as $E(2\omega) = C\chi_{MoS_2}^{(2)} \cos(3\phi + \phi_0)$ or $E(2\omega) = C\chi_{MoS_2}^{(2)} \sin(3\phi + \phi_0)$ respectively, where ϕ is the angle between the input laser polarization and the x direction and ϕ_0 is the initial crystallographic orientation of the MoS_2 sample. Hence the intensity of the generated SHG is proportional to $\cos^2(3\phi + \phi_0)$ (Fig. 2(e)). At maximum (minimum) of SHG intensity in parallel (perpendicular) configuration, the direction of polarization of input laser represents to armchair direction accordingly. With such relationship, polarized SHG has been widely used to characterize the crystal orientation for odd layers of 2H phases. While for other crystal forms of 2D materials belonging to different space groups, two-fold or four-fold pattern are employed as indicators of crystal orientation [40].

3. SHG characterization of 2D polar materials

Beyond transition metal dichalcogenide monolayers with intrinsic in-plane asymmetry, 2D polar materials with breaking out-of-plane mirror symmetry and finite vertical dipoles, are expected to have more degree of freedom for manipulation of spin and electrical properties [41,42]. Angle-dependent polarized SHG technique plays a significant role to characterize stable out-of-plane dipoles in both Janus structures [43] and out-of-plane 2D ferroelectric materials [44]. Janus MoSSe monolayers were first synthesized through replacing one atomic layer of S atom with H and then Se in sequence (Fig. 3(a)). The imbalance of S and Se atom, bonded with Mo atom in bottom and top, breaks the mirror symmetry and results in an out-of-plane dipole. Such atomic polar structure can be an important platform to study dipole-dipole correlations and strong coupling with plasmonic structures, characterization of its optical vertical dipole is necessary. To verify polar structure, researchers conducted polarization-selective SHG measurements with tilted-angle incidence (Fig. 3(b)). In this type of measurement, the *p*-polarized light pump and SHG detection were set perpendicular to Mo-X bond direction to minimize the contribution from the in-plane dipole. In the next, positioning the incident pump beam off-center at the back aperture of the microscope objective generates the tilted angle of incident beam at sample plane. With larger incident angle, the authors observed that the SHG intensity increase in the Janus MoSSe after an angle-dependent collection efficiency normalization (Fig. 3(c)). This is a signature of presence of out-of-plane optical dipole, which contributes more SHG emission with the stronger projected z-component of the field as the incident angle increases.

The same method was also used to characterize out-of-plane dipole in two-dimensional ferroelectric In_2Se_3. In a single layer of In_2Se_3, five layers of atoms stack through covalent bond as Se-In-Se-In-Se, which belongs to R_{3m} space group (Fig. 3(d)). The Se atom sits asymmetrically in the middle and breaks inversion symmetry, providing two degenerate states with opposite out-of-plane electric polarizations and second-order nonlinear polarization in plane. Since the depolarization field is large, there is a chance that ferroelectric order is not stable at low-dimensional limit [45,46]. The verification of the presence of the out-of-plane asymmetry at 2D limit becomes the first step for confirming ferroelectric order. Following the same process above, researchers first rotated the crystal to the SHG extinction point for in-plane nonlinear dipole contribution, where the In-Se bond direction is perpendicular to both the incident and detecting polarization direction. And then the tilting incident beam drives the out-of-plane dipole. As the tilt angle increases, SHG intensity increases as the z component of

Optical Materials EXPRESS

the optic electric field becomes stronger and is symmetric for positive and negative tilt angle. With this method, out-of-plane polarization in ferroelectric materials is preliminarily confirmed.

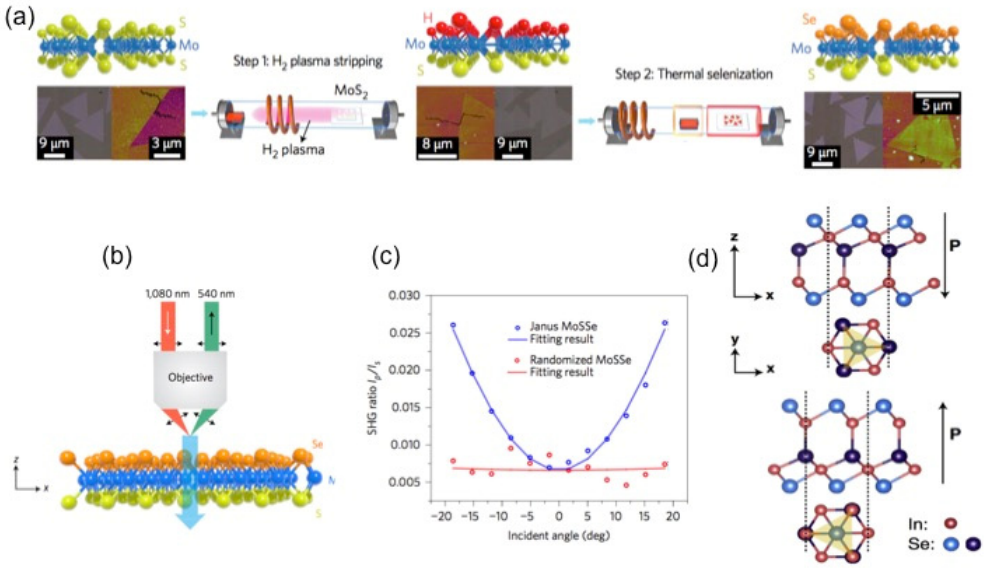

Fig. 3: (a) Synthesis of the Janus MoSSe monolayer. Optical microscopy and atomic force microscopy images are shown for each growth step. (b) Schematics of out-of-plane induced SHG. The beam position (red) at the objective back aperture can be scanned along the x direction with a motorized stage, which tunes the incident angle accordingly. The SHG (green) is collected by the same objective and analyzed by a polarizer. (c) Angle-dependent SHG intensity ratio between p and s polarization in the Janus MoSSe and randomized alloy samples. (d) Side view of two energy-degenerate ferroelectric In_2Se_3 structures. Single quintuple layer consists of covalently bonded indium and selenium triangular lattices. (a)-(c) are reprinted from ref [43] with permission from Springer Nature. (d) is adapted from ref [44] with permission from American Physical Society.

4. Large enhancement and tunability of SHG in two-dimensional materials

4.1 Large enhancement and tunability of SHG by excitonic effect

Monolayers of TMDs have large second-order nonlinear coefficients, which represent the efficiency of generating SHG. For example, the MoS_2 monolayer has an effective nonlinear susceptibility that is 1 order of magnitude larger than transparent nonlinear crystals and similar to absorbing ones [34]. Besides the large nonlinear coefficients, the strong excitonic effect in 2D materials makes them suitable for new generation of nonlinear photonics. When electrons and holes simultaneously exist in two-dimensional materials, they will form excitons even at room temperature due to the strong Coulomb interaction, which is enhanced by reduced dielectric screening and strong quantum confinement in 2D limit [47–49]. Excitons with strong bonding energy up to hundreds of meV form a series of excitonic Rydberg-like states similar to the hydrogen model [29,50]. The excited states of the bound electron-hole pairs are in series as 1*s*, 2*s*, 3*s*, and so on. This results in strong resonance effect in the absorption spectrum in monolayer TMDs, as shown in Fig. 4(a).

Optical Materials EXPRESS

Such resonance effect is under well control at 2D limit. People showed tuning the excitation on and off the excitonic resonance optically or electrically is an effective way to control the nonlinear response [51,52]. Firstly, through scanning the excitation energy across an exciton peak, the on-resonance SHG is over 15 times stronger than off the resonance, corresponding to a second-order susceptibility contrast of ~4 (Fig. 4(b)). More interestingly, the resonant SHG shows good tunability under electrical manipulation. People observed a nearly fourfold reduction in the resonant SHG intensity when gate voltage V_g is swept from −80 to 80V (Fig. 4(c)). And it is also found that larger carrier density, the smaller oscillator strength at the resonance. The origin of such tunability can be understood by the formation of positive and negative trions at high carrier density. Figure 4(d) presents a SHG intensity maps as a function of gate voltage and SHG emission energy under the 0.85 eV excitation at 30K. For V_g near −40 V, there is a peak around 1.74 eV. Toward higher positive V_g the feature is suppressed and a new peak appears around 1.71 eV. And for more negative V_g the SHG peak shifts to lower energy. And these peaks are assigned to be a neutral exciton (X^0) for the peak at 1.74 eV, negatively charged excitons (negative trions, X^-) near 1.71 eV at small positive V_g, and positive trions (X^+) at lower energy for high negative V_g (see in Fig. 4(e)). Since exciton and trion are eigenstates of Coulomb interaction at different doping level, the density of states as well as the optical oscillator strength shifts from exciton resonance to trion resonance as doping changes. Hence, the tuning of the SHG efficiency at a given energy is expected. Less screening in 2D materials widens the range of carrier density so that the large SHG intensity modulation is one unique feature for 2D materials.

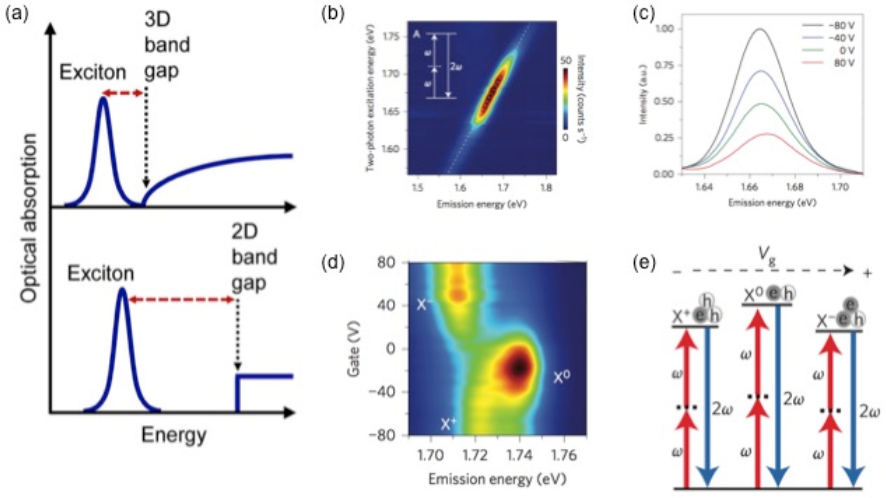

Fig. 4. (a) Schematics of the impact of the dimensionality on the electronic and excitonic properties, represented by optical absorption. The transition from 3D to 2D is expected to lead to an increase of both the band gap and the exciton binding energy. Reprinted from ref [50] with permission from American Physical Society. (b) Two-photon excitation map shows the strong SHG resonance. (c) SHG spectra on resonance with the exciton at selected gate biases. (d) SHG intensity maps as a function of gate voltage and emission energy. (e) Illustration of gate-dependent exciton- and trion-enhanced SHG. (b)-(e) are adapted from ref [52] with permission from Springer Nature.

Optical Materials EXPRESS

4.2 Large enhancement of SHG by integration with optical cavity

Multiple layer transfer methods, controlling the process of stacking one material onto another, have been well developed. Such progress makes the integration of various materials become accessible. Integration of 2D materials with well-designed optical cavity to form hybrid systems have been used to enhance the nonlinear coefficient or lower the switch power for the nonlinear optical process. For example, people put a monolayer of WSe_2 on the top of a silicon photonic cavity and increase the SHG intensity by 200 times, compared to the bare monolayer [53] (Fig. 5(a) and 5(b)). Essentially, silicon with centrosymmetry results in the lack of second order nonlinearity and hinders the application of second order nonlinear integrated photonics. But silicon-based photonic crystal cavity is proved to have both small mode volume (V_m) and high quality factor (Q), where light can be confined and exist for an extended period of time [54,55]. And the switching power for second order nonlinearity is proportional to V_mQ^3. After transferring the monolayer WSe_2, the Q of three-hole linear defect photonic crystal cavity (PCC) is ~700-800 and two resonances (~1490 nm and ~1515 nm) of the 2D integrated cavity were observed in the reflectance measurement (Fig. 5(c)), trapping more light for SHG excitation. And the observed SHG signal (~745 nm and ~758 nm) correspond exactly to the half of the cavity resonances (~1490 nm and ~1515 nm) (see in Fig. 5(d)), which is the evidence for enhancement from cavity. Comparing the SHG peak intensity and the power coupled into the cavity, the nonlinear conversion efficiency is estimated to be ~1%. And in contrast to such efficiency for bare monolayers, the cavity enhancement is found to be ~200 at the lowest pump power and opens the door to energy-efficient nonlinear photonics. More recently, with the ultrahigh second order nonlinearity of GaSe and extremely confined resonant mode of the cavity, efficient SHGs in GaSe flakes with an CW excitation power less than 10 μW [56]. The enhancement factor is estimated over 650. Furthermore, based on the similar material and device system, multiple second□order nonlinear processes such as sum frequency generations (SFGs) and cascaded SFGs have been demonstrated [57]. These findings promise the energy-efficient ultrathin optoelectronic devices in nonlinear regime.

Optical Materials EXPRESS

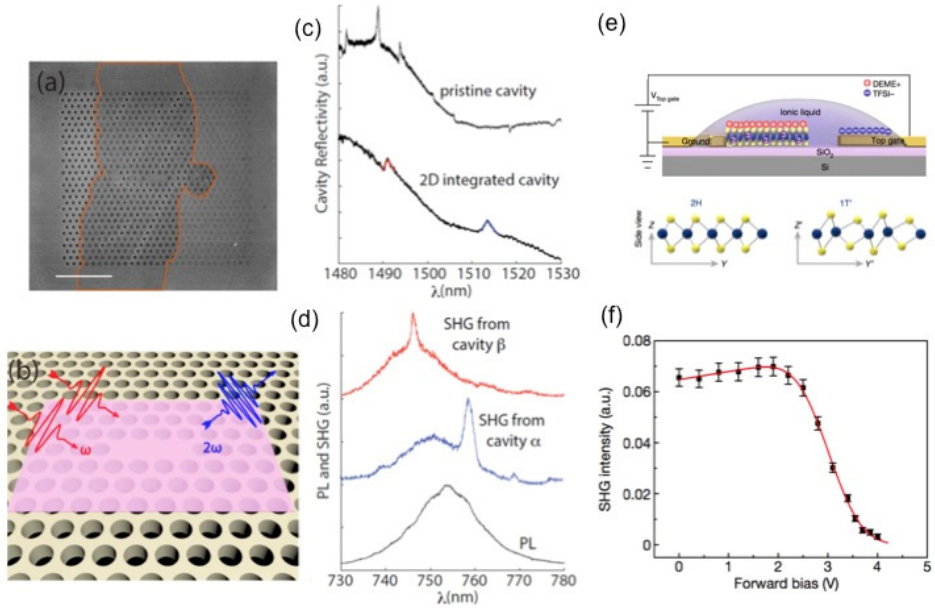

Fig. 5. (a) Scanning electron micrograph of the fabricated silicon photonic crystal cavity with monolayer WSe_2 on top, indicated by the orange outline. Scale bar: 10μm. (b) Schematic of the device operation: two infrared (IR) photons with frequency ω (in red) resonantly couple into the photonic crystal cavity. The cavity mode interacts with the WSe_2 (the transparent pink sheet), which then generates the second harmonic photon at a frequency of 2ω (in blue). (c) Cross-polarized reflectivity measurements of the higher order cavity modes before and after monolayer WSe_2 transfer. The mode 'α' at ~1515 nm and the mode 'β' at ~1490 nm are highlighted in blue and red respectively 'β' at ~1490 nm. (d) Overlay of the photoluminescence signal from WSe_2 generated via a HeNe laser (black), SHG spectrum from mode α (blue), and SHG spectrum from mode β (red). (e) Schematics and measurement configuration of a $MoTe_2$ monolayer field-effect transistor with ionic liquid gate, through which 2H phase can be converted into 1T' phase via gating. Crystal structures of the 2H and 1T′ phases of monolayer $MoTe_2$ are shown in the inset. (e) Typical SHG intensity modulation for this monolayer while phase changes from 2H to 1T'. (a)-(d) are reprinted from ref [53] with permission from IOP Publishing. (e)-(f) are reprinted with from ref [58] with permission from Springer Nature.

4.3 SHG modulation through phase transition

More recently, different phases of crystals can be obtained due to the small energy difference between each of them. For instance, 2H and 1T' phases are two possible phases for $MoTe_2$ and exhibit giant difference in physical properties, including symmetries. People demonstrated phase transition in a $MoTe_2$ transistor via electrostatic doping, accompanying with symmetry change (Fig. 5(e)) [58]. In principle through gate bias, the excessive electrons are injected into a monolayer of the 2H phase and occupy the lowest available energy states in the conduction band, which are hundreds of milli-electron volts higher than that in the 1T′ phase. Therefore, at high doping levels, the extra electrons are expected to carry enough energy to lift the total energy of the 2H phase above that of the 1T′ phase, switching the ground state from 2H to 1T′ and inducing a structural phase transition [59]. Along with phase change, the finite SHG vanishes due to the centrosymmetry in the doping-induced monolayer 1T' phase (Fig. 5(f)). Meanwhile, 2H phase of $MoTe_2$ shows the largest nonlinear coefficient among all of the 2D materials [60] and hence gives a good modulation depth of SHG intensity

Optical Materials EXPRESS

while phase changes. Moreover, the polarized SHG can be a supplemental tool to distinguish crystal phases in few layers. Unlike the six fold pattern observed in 2H phase, two-fold pattern is found in 1T' few-layer crystal because it belongs to C_s^1 space group [60]. Furthermore, with the assist of pump-probe SHG, it is a chance to exhibit evolution and dynamics of phase transitions at 2D limit in the near future.

5. Conclusion and outlook

In conclusion, SHG spectroscopy and microscopy have been widely applied in research on 2D materials, which reveal multiple advantages such as sensitivity to crystal symmetry, non-contact and non-invasive, free of fabrication and easy operation. We have mainly reviewed its application in characterization of crystal orientation and boundary, detection of structural phase transition and discovery of asymmetric polar materials with out-of-plane piezoelectricity or ferroelectricity. On the other hand, 2D materials in turn have revealed huge potentials to develop 2D nonlinear optical device applications with new functionalities based on their giant nonlinear coefficients, strong excitonic enhancement and large electrical tunablity. Clearly, application of SHG spectroscopy and microscopy on atomically thin layered materials provide an easy yet versatile way for exploring novel physics and enables the development of diverse devices derived from these materials.

Current research progress also points towards several future directions. For example, SHG characterization of emerging 2D magnetic materials is in urgent need. Indeed, SHG has been used to detect magnetic ordering demonstrated by early studies [61–65]. Especially SHG is powerful in the case of AFs where linear MOKE effects are rather weak. Alternatively, SHG can be employed to probe the pump-induced dynamics [66–69]. For 2D layered materials, multiple types of magnetic orderings were reported recently including ferromagnetism and antiferromagnetism [70]. Probing magnetic ordering formation, magnetic domain and ultrafast magnetic dynamics by SHG is still in its infancy. Another opportunity lies in SHG application on topological Weyl semimetal. One type of Weyl semimetal is based on inversion symmetry breaking such as TaAs [71] (Type I) and Td-phase MTe2 [72] (M = Mo, W, Type II). Besides their novel topological properties and potential applications in spintronics and quantum information, their breaking inversion symmetry features can be easily probed by SHG as recently demonstrated [73]. What's more, the diverging berry curvature close to Weyl points lead to giant SHG enhancement, which may enable topological nonlinear optical devices. Further exploration on this topic to link SHG with topology and Berry curvature is waiting. Finally, while this review focuses on experimental part of SHG researches in 2D materials, it is worthwhile for researchers to investigate theoretical modeling of SHG in 2D materials as well [74,75]. For example, one open question is how to comprehensively include the important substrate effect into the modeling of SHG in 2D materials. For atomically thin crystals, the interface and substrate naturally become significant. The photonic boundary conditions, the mechanical strain, the electrical charge transfer and other interfacial factors need to be suitably modeled and explored in the future.

Funding

National Science Foundation (EFMA-1542741); King Abdullah University of Science and Technology (KAUST) Office of Sponsored Research (OSR) (OSR-2016-CRG5-2996).

References

1. Y. Zhang, Y. W. Tan, H. L. Stormer, and P. Kim, "Experimental observation of the quantum Hall effect and Berry's phase in graphene," Nature **438**(7065), 201–204 (2005).
2. S. Ghosh, I. Calizo, D. Teweldebrhan, E. P. Pokatilov, D. L. Nika, A. A. Balandin, W. Bao, F. Miao, and C. N. Lau, "Extremely high thermal conductivity of graphene: Prospects for thermal management applications in nanoelectronic circuits," Appl. Phys. Lett. **92**, 151911 (2008).
3. A. H. Castro Neto, F. Guinea, N. M. R. Peres, K. S. Novoselov, and A. K. Geim, "The electronic properties of graphene," Rev. Mod. Phys. **81**(1), 109–162 (2009).
4. C. Gong, L. Li, Z. Li, H. Ji, A. Stern, Y. Xia, T. Cao, W. Bao, C. Wang, Y. Wang, Z. Q. Qiu, R. J. Cava, S. G.

Optical Materials EXPRESS

Louie, J. Xia, and X. Zhang, "Discovery of intrinsic ferromagnetism in two-dimensional van der Waals crystals," Nature **546**(7657), 265–269 (2017).
5. S. Z. Butler, S. M. Hollen, L. Cao, Y. Cui, J. A. Gupta, H. R. Gutiérrez, T. F. Heinz, S. S. Hong, J. Huang, A. F. Ismach, E. Johnston-Halperin, M. Kuno, V. V. Plashnitsa, R. D. Robinson, R. S. Ruoff, S. Salahuddin, J. Shan, L. Shi, M. G. Spencer, M. Terrones, W. Windl, and J. E. Goldberger, "Progress, challenges, and opportunities in two-dimensional materials beyond graphene," ACS Nano **7**(4), 2898–2926 (2013).
6. X. Duan, C. Wang, A. Pan, R. Yu, and X. Duan, "Two-dimensional transition metal dichalcogenides as atomically thin semiconductors: opportunities and challenges," Chem. Soc. Rev. **44**(24), 8859–8876 (2015).
7. D. Jariwala, V. K. Sangwan, L. J. Lauhon, T. J. Marks, and M. C. Hersam, "Emerging device applications for semiconducting two-dimensional transition metal dichalcogenides," ACS Nano **8**(2), 1102–1120 (2014).
8. Q. H. Wang, K. Kalantar-Zadeh, A. Kis, J. N. Coleman, and M. S. Strano, "Electronics and optoelectronics of two-dimensional transition metal dichalcogenides," Nat. Nanotechnol. **7**(11), 699–712 (2012).
9. B. Radisavljevic, A. Radenovic, J. Brivio, V. Giacometti, and A. Kis, "Single-layer MoS_2 transistors," Nat. Nanotechnol. **6**(3), 147–150 (2011).
10. T. Cao, G. Wang, W. Han, H. Ye, C. Zhu, J. Shi, Q. Niu, P. Tan, E. Wang, B. Liu, and J. Feng, "Valley-selective circular dichroism of monolayer molybdenum disulphide," Nat. Commun. **3**(1), 887 (2012).
11. H. Zeng, J. Dai, W. Yao, D. Xiao, and X. Cui, "Valley polarization in MoS_2 monolayers by optical pumping," Nat. Nanotechnol. **7**(8), 490–493 (2012).
12. K. F. Mak, K. L. McGill, J. Park, and P. L. McEuen, "Valleytronics. The valley Hall effect in MoS□ transistors," Science **344**(6191), 1489–1492 (2014).
13. X. Zhang, Q. H. Tan, J. B. Wu, W. Shi, and P. H. Tan, "Review on the Raman spectroscopy of different types of layered materials," Nanoscale **8**(12), 6435–6450 (2016).
14. W. Zhao, Z. Ghorannevis, L. Chu, M. Toh, C. Kloc, P.-H. Tan, and G. Eda, "Evolution of electronic structure in atomically thin sheets of WS_2 and WSe_2," ACS Nano **7**(1), 791–797 (2013).
15. Y. Li, A. Chernikov, X. Zhang, A. Rigosi, H. M. Hill, A. M. Van Der Zande, D. A. Chenet, E.-M. Shih, J. Hone, and T. F. Heinz, "Measurement of the optical dielectric function of monolayer transition-metal dichalcogenides: MoS_2, $MoSe_2$, WS_2, and WSe," Phys. Rev. B **90**, 205422 (2014).
16. K. F. Mak, C. Lee, J. Hone, J. Shan, and T. F. Heinz, "Atomically thin MoS□: a new direct-gap semiconductor," Phys. Rev. Lett. **105**(13), 136805 (2010).
17. S. Zhang, J. Yang, R. Xu, F. Wang, W. Li, M. Ghufran, Y. W. Zhang, Z. Yu, G. Zhang, Q. Qin, and Y. Lu, "Extraordinary photoluminescence and strong temperature/angle-dependent Raman responses in few-layer phosphorene," ACS Nano **8**(9), 9590–9596 (2014).
18. X. Wang, A. M. Jones, K. L. Seyler, V. Tran, Y. Jia, H. Zhao, H. Wang, L. Yang, X. Xu, and F. Xia, "Highly anisotropic and robust excitons in monolayer black phosphorus," Nat. Nanotechnol. **10**(6), 517–521 (2015).
19. K. S. Novoselov, A. Mishchenko, A. Carvalho, A. H. Castro Neto, and O. Road, "2D materials and van der Waals heterostructures," Science **353**(6298), aac9439 (2016).
20. A. K. Geim and I. V. Grigorieva, "Van der Waals heterostructures," Nature **499**(7459), 419–425 (2013).
21. X. Wang and F. Xia, "Van der Waals heterostructures: Stacked 2D materials shed light," Nat. Mater. **14**(3), 264–265 (2015).
22. Y. R. Shen, "Surface properties probed by second-harmonic and sum-frequency generation," Nature **337**(6207), 519–525 (1989).
23. Y. G. Fokin, T. V. Murzina, O. A. Aktsipetrov, S. Soria, and G. Marowsky, "Phase transitions in ferroelectric liquid crystals probed by optical second harmonic generation" Surf. Sci. **507-510**, 724–729 (2002).
24. M. Zhao, Z. Ye, R. Suzuki, Y. Ye, H. Zhu, J. Xiao, Y. Wang, Y. Iwasa, and X. Zhang, "Atomically phase-matched second-harmonic generation in a 2D crystal," Light Sci. Appl. **5**(8), e16131 (2016).
25. L. M. Malard, T. V. Alencar, A. P. M. Barboza, K. F. Mak, and A. M. De Paula, "Observation of intense second harmonic generation from Mo_2 atomic crystals," Phys. Rev. B Condens. Matter Mater. Phys. **87**, 801401 (2013).
26. K. F. Mak, C. Lee, J. Hone, J. Shan, and T. F. Heinz, "Atomically thin MoS□: a new direct-gap semiconductor," Phys. Rev. Lett. **105**, 136805 (2010).
27. A. Splendiani, L. Sun, Y. Zhang, T. Li, J. Kim, C. Y. Chim, G. Galli, and F. Wang, "Emerging photoluminescence in monolayer MoS_2," Nano Lett. **10**(4), 1271–1275 (2010).
28. K. F. Mak, K. He, J. Shan, and T. F. Heinz, "Control of valley polarization in monolayer MoS_2 by optical helicity," Nat. Nanotechnol. **7**(8), 494–498 (2012).
29. Z. Ye, T. Cao, K. O'Brien, H. Zhu, X. Yin, Y. Wang, S. G. Louie, and X. Zhang, "Probing excitonic dark states in single-layer tungsten disulphide," Nature **513**(7517), 214–218 (2014).
30. K. F. Mak, K. He, C. Lee, G. H. Lee, J. Hone, T. F. Heinz, and J. Shan, "Tightly bound trions in monolayer MoS_2," Nat. Mater. **12**, 207 (2013).
31. J. T. Ye, Y. J. Zhang, R. Akashi, M. S. Bahramy, R. Arita, and Y. Iwasa, "Superconducting dome in a gate-tuned band insulator," Science **338**, 1193 (2012).
32. H. Zhu, Y. Wang, J. Xiao, M. Liu, S. Xiong, Z. J. Wong, Z. Ye, Y. Ye, X. Yin, and X. Zhang, "Observation of piezoelectricity in free-standing monolayer MoS□," Nat. Nanotechnol. **10**(2), 151–155 (2015).
33. W. Wu, L. Wang, Y. Li, F. Zhang, L. Lin, S. Niu, D. Chenet, X. Zhang, Y. Hao, T. F. Heinz, J. Hone, and Z. L. Wang, "Piezoelectricity of single-atomic-layer MoS_2 for energy conversion and piezotronics," Nature **514**(7523), 470–474 (2014).
34. Y. Li, Y. Rao, K. F. Mak, Y. You, S. Wang, C. R. Dean, and T. F. Heinz, "Probing symmetry properties of few-

Optical Materials EXPRESS

layer MoS_2 and h-BN by optical second-harmonic generation," Nano Lett. **13**(7), 3329–3333 (2013).
35. Y. Song, S. Hu, M. L. Lin, X. Gan, P. H. Tan, and J. Zhao, "Extraordinary Second Harmonic Generation in ReS_2 Atomic Crystals," ACS Photonics **5**(9), 3485–3491 (2018).
36. K. Kim, S. Coh, L. Z. Tan, W. Regan, J. M. Yuk, E. Chatterjee, M. F. Crommie, M. L. Cohen, S. G. Louie, and A. Zettl, "Raman Spectroscopy Study of Rotated Double-Layer Graphene: Misorientation-Angle Dependence of Electronic Structure," Phys. Rev. Lett. **108**, 246103 (2012).
37. L. Kou, T. Frauenheim, and C. Chen, "Nanoscale Multilayer Transition-Metal Dichalcogenide Heterostructures: Band Gap Modulation by Interfacial Strain and Spontaneous Polarization," J. Phys. Chem. Lett. **4**(10), 1730–1736 (2013).
38. W. T. Hsu, Z. A. Zhao, L. J. Li, C. H. Chen, M. H. Chiu, P. S. Chang, Y. C. Chou, and W. H. Chang, "Second harmonic generation from artificially stacked transition metal dichalcogenide twisted bilayers," ACS Nano **8**(3), 2951–2958 (2014).
39. X. Yin, Z. Ye, D. A. Chenet, Y. Ye, K. O'Brien, J. C. Hone, and X. Zhang, "Edge nonlinear optics on a MoS_2 atomic monolayer," Science **344**(6183), 488–490 (2014).
40. R. Beams, L. G. Cançado, S. Krylyuk, I. Kalish, B. Kalanyan, A. K. Singh, K. Choudhary, A. Bruma, P. M. Vora, F. Tavazza, A. V. Davydov, and S. J. Stranick, "Characterization of Few-Layer 1T′ $MoTe_2$ by Polarization-Resolved Second Harmonic Generation and Raman Scattering," ACS Nano **10**(10), 9626–9636 (2016).
41. H. Yuan, M. S. Bahramy, K. Morimoto, S. Wu, K. Nomura, B. J. Yang, H. Shimotani, R. Suzuki, M. Toh, C. Kloc, X. Xu, R. Arita, N. Nagaosa, and Y. Iwasa, "Zeeman-type spin splitting controlled by an electric field," Nat. Phys. **9**(9), 563–569 (2013).
42. S. Wu, J. S. Ross, G. Bin Liu, G. Aivazian, A. Jones, Z. Fei, W. Zhu, D. Xiao, W. Yao, D. Cobden, and X. Xu, "Electrical tuning of valley magnetic moment through symmetry control in bilayer MoS_2," Nat. Phys. **9**(3), 149–153 (2013).
43. A.-Y. Lu, H. Zhu, J. Xiao, C.-P. Chuu, Y. Han, M.-H. Chiu, C.-C. Cheng, C.-W. Yang, K.-H. Wei, Y. Yang, Y. Wang, D. Sokaras, D. Nordlund, P. Yang, D. A. Muller, M.-Y. Chou, X. Zhang, and L.-J. Li, "Janus monolayers of transition metal dichalcogenides," Nat. Nanotechnol. **12**, 744 (2017).
44. J. Xiao, H. Zhu, Y. Wang, W. Feng, Y. Hu, A. Dasgupta, Y. Han, Y. Wang, D. A. Muller, L. W. Martin, P. Hu, and X. Zhang, "Intrinsic Two-Dimensional Ferroelectricity with Dipole Locking," Phys. Rev. Lett. **120**, 227601 (2018).
45. E. A. Eliseev, S. V. Kalinin, and A. N. Morozovska, "Finite size effects in ferroelectric-semiconductor thin films under open-circuit electric boundary conditions," J. Appl. Phys. **117**(3), 034102 (2015).
46. J. Junquera and P. Ghosez, "Critical thickness for ferroelectricity in perovskite ultrathin films," Nature **422**(6931), 506–509 (2003).
47. K. He, N. Kumar, L. Zhao, Z. Wang, K. F. Mak, H. Zhao, and J. Shan, "Tightly Bound Excitons in Monolayer WSe_2," Phys. Rev. Lett. **113**, 026803 (2014).
48. A. R. Klots, A. K. M. Newaz, B. Wang, D. Prasai, H. Krzyzanowska, J. Lin, D. Caudel, N. J. Ghimire, J. Yan, B. L. Ivanov, K. A. Velizhanin, A. Burger, D. G. Mandrus, N. H. Tolk, S. T. Pantelides, and K. I. Bolotin, "Probing excitonic states in suspended two-dimensional semiconductors by photocurrent spectroscopy," Sci. Rep. **4**, 6608 (2014).
49. M. M. Ugeda, A. J. Bradley, S. F. Shi, F. H. da Jornada, Y. Zhang, D. Y. Qiu, W. Ruan, S. K. Mo, Z. Hussain, Z. X. Shen, F. Wang, S. G. Louie, and M. F. Crommie, "Giant bandgap renormalization and excitonic effects in a monolayer transition metal dichalcogenide semiconductor," Nat. Mater. **13**(12), 1091–1095 (2014).
50. A. Chernikov, T. C. Berkelbach, H. M. Hill, A. Rigosi, Y. Li, O. B. Aslan, D. R. Reichman, M. S. Hybertsen, and T. F. Heinz, "Exciton binding energy and nonhydrogenic Rydberg series in monolayer WS_2," Phys. Rev. Lett. **113**(7), 076802 (2014).
51. G. Wang, X. Marie, I. Gerber, T. Amand, D. Lagarde, L. Bouet, M. Vidal, A. Balocchi, and B. Urbaszek, "Giant Enhancement of the Optical Second-Harmonic Emission of WSe_2 Monolayers by Laser Excitation at Exciton Resonances," Phys. Rev. Lett. **114**, 097403 (2015).
52. K. L. Seyler, J. R. Schaibley, P. Gong, P. Rivera, A. M. Jones, S. Wu, J. Yan, D. G. Mandrus, W. Yao, and X. Xu, "Electrical control of second-harmonic generation in a WSe_2 monolayer transistor," Nat. Nanotechnol. **10**(5), 407–411 (2015).
53. T. K. Fryett, K. L. Seyler, J. Zheng, C. H. Liu, X. Xu, and A. Majumdar, "Silicon photonic crystal cavity enhanced second-harmonic generation from monolayer WSe_2," 2D Mater. **4**, 1 (2017).
54. K. J. Vahala, "Optical microcavities," Nature **424**(6950), 839–846 (2003).
55. R. Trivedi, U. K. Khankhoje, and A. Majumdar, "Cavity-Enhanced Second-Order Nonlinear Photonic Logic Circuits," Phys. Rev. Appl. **5**(5), 54001 (2015).
56. X. T. Gan, C. Y. Zhao, S. Q. Hu, T. Wang, Y. Song, J. Li, Q. H. Zhao, W. Q. Jie, and J. L. Zhao, "Microwatts continuous-wave pumped second harmonic generation in few- and mono-layer GaSe," Light Sci. Appl. **7**, 17126 (2018).
57. L. Fang, Q. Yuan, H. Fang, X. Gan, J. Li, T. Wang, Q. Zhao, W. Jie, and J. Zhao, Adv. Opt. Mater. **6**, (2018).
58. Y. Wang, J. Xiao, H. Zhu, Y. Li, Y. Alsaid, K. Y. Fong, Y. Zhou, S. Wang, W. Shi, Y. Wang, A. Zettl, E. J. Reed, and X. Zhang, "Structural phase transition in monolayer $MoTe_2$ driven by electrostatic doping," Nature **550**(7677), 487 (2017).
59. Y. Li, K.-A. N. Duerloo, K. Wauson, and E. J. Reed, "Structural semiconductor-to-semimetal phase transition in

Optical Materials EXPRESS

two-dimensional materials induced by electrostatic gating," Nat. Commun. **7**(1), 10671 (2016).
60. Y. Song, R. Tian, J. Yang, R. Yin, J. Zhao, and X. Gan, "Second Harmonic Generation in Atomically Thin $MoTe_2$," Adv. Opt. Mater. **6**(17), 1701334 (2018).
61. M. Fiebig, D. Fröhlich, B. B. Krichevtsov, and R. V. Pisarev, "Second harmonic generation and magnetic-dipole-electric-dipole interference in antiferromagnetic Cr_2O_3," Phys. Rev. Lett. **73**(15), 2127–2130 (1994).
62. J. Reif, J. C. Zink, C.-M. Schneider, and J. Kirschner, "Effects of surface magnetism on optical second harmonic generation," Phys. Rev. Lett. **67**, 2878 (1991).
63. J. Reif, C. Rau, and E. Matthias, "Influence of magnetism on second harmonic generation," Phys. Rev. Lett. **71**(12), 1931–1934 (1993).
64. M. Fiebig, V. V. Pavlov, and R. V. Pisarev, "Second-harmonic generation as a tool for studying electronic and magnetic structures of crystals: review," J. Opt. Soc. Am. B **22**(1), 96 (2005).
65. M. Fiebig, T. Lottermoser, D. Fröhlich, and S. Kallenbach, "Phase-resolved second-harmonic imaging with nonideal laser sources," Opt. Lett. **29**(1), 41–43 (2004).
66. S. Manz, M. Matsubara, T. Lottermoser, J. Büchi, A. Iyama, T. Kimura, D. Meier, and M. Fiebig, "Reversible optical switching of antiferromagnetism in $TbMnO_3$," Nat. Photonics **10**(10), 653–656 (2016).
67. M. Fiebig, N. P. Duong, and T. Satoh, in *Conf. Lasers Electro-Optics 2006 Quantum Electron. Laser Sci. Conf. CLEO/QELS 2006* (2006).
68. A. Rubano, T. Satoh, A. Kimel, A. Kirilyuk, T. Rasing, and M. Fiebig, "Influence of laser pulse shaping on the ultrafast dynamics in antiferromagnetic NiO," Phys. Rev. B Condens. Matter Mater. Phys. **82**(17), 174431 (2010).
69. D. Afanasiev, B. A. Ivanov, A. Kirilyuk, T. Rasing, R. V. Pisarev, and A. V. Kimel, "Control of the Ultrafast Photoinduced Magnetization across the Morin Transition in $DyFeO_3$," Phys. Rev. Lett. **116**, 097401 (2016).
70. Editorial, "2D magnetism gets hot," Nat. Nanotechnol. **13**, 269 (2018).
71. B. Q. Lv, H. M. Weng, B. B. Fu, X. P. Wang, H. Miao, J. Ma, P. Richard, X. C. Huang, L. X. Zhao, G. F. Chen, Z. Fang, X. Dai, T. Qian, and H. Ding, "Experimental Discovery of Weyl Semimetal TaAs," Phys. Rev. X **5**, 031013 (2015).
72. A. A. Soluyanov, D. Gresch, Z. Wang, Q. Wu, M. Troyer, X. Dai, and B. A. Bernevig, "Type-II Weyl semimetals," Nature **527**(7579), 495–498 (2015).
73. L. Wu, S. Patankar, T. Morimoto, N. L. Nair, E. Thewalt, A. Little, J. G. Analytis, J. E. Moore, and J. Orenstein, "Giant anisotropic nonlinear optical response in transition metal monopnictide Weyl semimetals," Nat. Phys. **13**(4), 350–355 (2017).
74. S. Hong, J. I. Dadap, N. Petrone, P. Yeh, J. Hone, and R. M. Osgood, "Optical Third-Harmonic Generation in Graphene," Phys. Rev. X **3**(2), 021014 (2013).
75. M. Merano, "Nonlinear optical response of a two-dimensional atomic crystal," Opt. Lett. **41**(1), 187–190 (2016).